MRS BULLETIN

Serving the International Materials Research Community

A Publication of the Materials Research Society

May 1995, Volume XX, No. 5

In Situ, Real-Time Characterization of Thin-Film Growth Processes

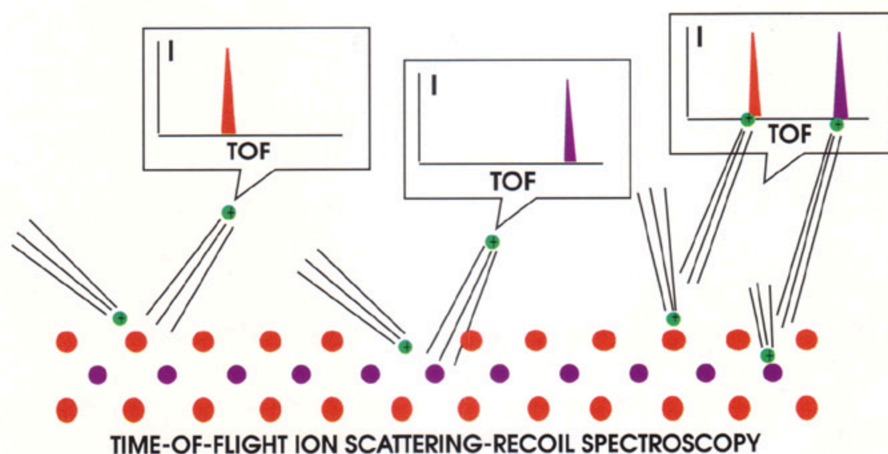

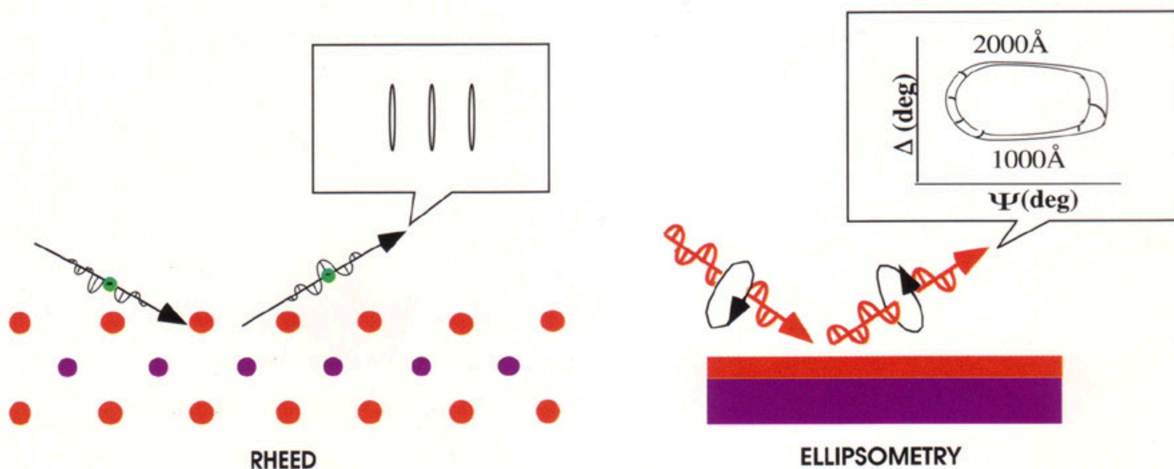

Real-Time Monitoring of Epitaxial Processes by Parallel-Polarized Reflectance Spectroscopy

Nikolaus Dietz and Klaus J. Bachmann

Introduction

The engineering of advanced microelectronic circuits, optoelectronic devices, and integrated optical circuits requires precise control of the lateral dimensions and thicknesses of device features and of the stoichiometry and doping of epitaxial semiconductor regions. This is preferably achieved by real-time monitoring and control of the individual deposition and etching processes that constitute the processing sequence. The use of optical probe techniques for the real-time monitoring of etching and/or growth processes is favored because of their nondestructive character and their potential use in real-time feedback control. Some of these methods are ideal in monitoring the overall growth process and/or substrate temperature in industrial applications, requiring low cost and maintenance. For example, *in situ* reflectance-spectroscopy methods, such as dynamic optical reflectivity (DOS),[1] spectral-resolved normal incidence reflectance spectroscopy (NIRS),[2] or pyrometric interferometry (PI),[3] are successfully applied to various deposition processes and provide information on both the growth rate and the composition of the deposits. However, small changes in the reflectance (because of chemical interactions at the surface of the films with the reactants supplied from the vapor phase) are of the order of 10^{-3} to 10^{-4} and are hardly observable with normal-incidence reflectance techniques because of the high reflectivity of substrate/film interface, which is typically of the order of 40%–60% for many semiconductors.

In order to increase the sensitivity to surface- and interface-related growth properties, alternative optical-observation methods such as reflectance difference spectroscopy (RDS),[4,5] surface photoabsorption (SPA),[6,7] and spectral ellipsometry (SE)[8,9] have been developed. Recently, we added to these methods a new optical probe technique, parallel-polarized reflectance spectroscopy (PRS), which achieves both high sensitivity to surface-chemistry processes and control of film thickness with submonolayer resolution. For example, we have shown that the real-time monitoring (by PRS) of the epitaxial overgrowth of Si by GaP, under the conditions of pulsed chemical beam epitaxy (PCBE), provides valuable insights into the mechanism of nucleation and follows the growth process with submonolayer resolution over thousands of angstroms of film growth.[10–13]

Model Considerations

A schematic representation of PRS is shown in Figure 1. When a monochromatic beam of parallel-polarized (p-polarized) light (e.g., light which is polarized parallel to the plane of incidence) impinges on an isotropic substrate surface at the Brewster angle φ_B, the intensity of the reflected light is zero for a dielectric medium and a minimum for an absorbing medium. In a simplified description, an isotropic dielectric substrate may be viewed as a second polarization element, crossed to the polarizer, resulting in zero reflectance R_p. To describe absorbing media, the Brewster angle law has to be modified from the condition $R_p = 0$ to a reflectance minimum condition $dR_p/d\varphi = 0$.[14] The angle of incidence at which the latter condition is satisfied is called the pseudo-Brewster or first Brewster angle. It can be defined analytically in terms of the complex dielectric function of an absorbing medium.[15]

The presence of a film for a material possessing a different dielectric function on top of the substrate modifies the Brewster angle condition and results in a shift in the angle φ_B and in an offset in

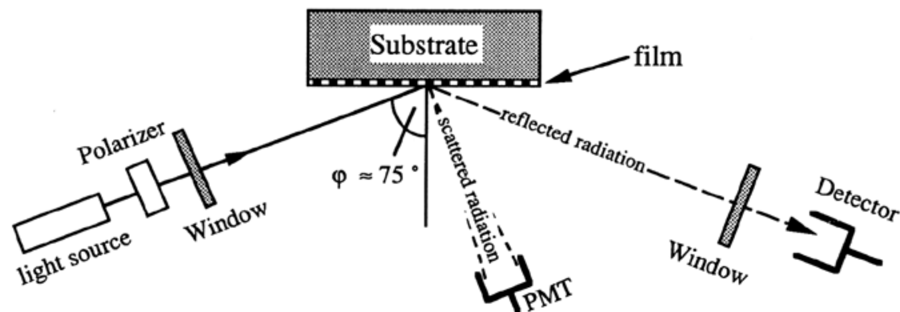

Figure 1. Schematic presentation of PRS.

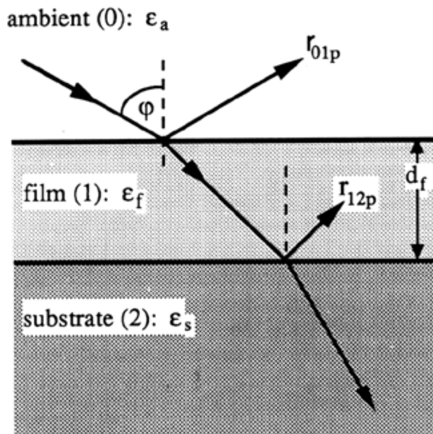

Figure 2. Model description of a three-layer system (ambient/film/substrate, assuming homogenous, isotropic, optical properties and a light source) which is p-polarized to the plane of incidence. φ is the angle of incidence, and d_f is the film thickness. ε_a, ε_f, and ε_s are the complex dielectric functions of the ambient, the film, and the substrate, respectively.

the reflectivity at φ_B. In order to describe the reflection of p-polarized light on the three-layer (ambient (e.g., air or vacuum)/film/substrate) stack presented in Figure 2, Fresnel's equations are used to calculate the changes of the reflectivity as a function of layer thickness,[16] assuming homogenous isotropic media. Labeling the media forming the stack a for ambient, f for film, and s for substrate, with interfaces labeled af and fs, the complex reflectance amplitude rr_p is given by

$$rr_p = \frac{r_{af_p} + r_{fs_p} \cdot e^{-2i\phi}}{1 + r_{af_p} \cdot r_{fs_p} \cdot e^{-2i\phi}} \quad (1)$$

with reflectance coefficients as a function of dielectric constants ε

$$r_{af_p} = \frac{\varepsilon_f \cos\varphi_0 - \sqrt{\varepsilon_a}\sqrt{\varepsilon_f - \varepsilon_a \sin^2\varphi_0}}{\varepsilon_f \cos\varphi_0 + \sqrt{\varepsilon_a}\sqrt{\varepsilon_f - \varepsilon_a \sin^2\varphi_0}} \quad (2a)$$

$$r_{fs_p} = \frac{\varepsilon_s\sqrt{\varepsilon_f - \varepsilon_a \sin^2\varphi_0} - \varepsilon_f\sqrt{\varepsilon_s - \varepsilon_a \sin^2\varphi_0}}{\varepsilon_s\sqrt{\varepsilon_f - \varepsilon_a \sin^2\varphi_0} + \varepsilon_f\sqrt{\varepsilon_s - \varepsilon_a \sin^2\varphi_0}} \quad (2b)$$

and phase factor

$$\Phi = \frac{2\pi d_f}{\lambda}\sqrt{\varepsilon_f - \varepsilon_a \sin^2\varphi_0} \quad (3)$$

where d_f is the film thickness.

In order to model the growth of a film, the reflectivity $R = rr_p \times rr_p^*$ has to be calculated as a function of film thickness and the complex dielectric function of the layer. A detailed evaluation of the Brewster angle and reflectivity shifts for the deposition of SiO_2 on an Si substrate is given by Azzam et al.[17] Calculations of the reflectivity as a function of film thickness and complex dielectric function show minima and maxima with a modulation in the reflectivity that is related to the differences of the dielectric functions of the substrate and of the growing film. One oscillation corresponds to a quarter-wave film thickness, taking into account the dielectric function of the film and the angle of incidence. Choosing the angle of incidence as the Brewster angle of the substrate results in zero reflectivity at the beginning of the growth process for a dielectric medium and a reflectivity close to the minimum for an absorbing medium. For example, the calculations predict changes of three orders of magnitude in the reflectance during GaP film growth on a Si substrate ($\varepsilon_{1(GaP)} \approx 10$, $\varepsilon_{1(Si)} \approx 15.25$), with a quarter-wave oscillation every 1050 Å. For a larger difference in the dielectric functions between film and substrate, as for example, in Si-oxide/Si heterostructures ($\varepsilon_{1(SiO2)} \approx 3, \varepsilon_{1(Si)} \approx 15.25$), the changes in the reflectance increases up to five orders of magnitude during film growth.[16]

The Fresnel equations also can be applied to describe changes in the reflectivity for multiple heterostructures assuming homogenous isotropic properties. For p-polarized light, no perpendicular reflectance component r_s has to be considered because only the parallel reflectance component r_p contributes to the reflectance amplitude. For brevity, the index p in the following text will be dropped. For an n layer stack, ambient/film 1/ ... /film n/substrate (as schematically shown in Figure 3), the reflectance coefficient from the $(n-1)^{th}$ to the nth layer $r_{(n-1)n}$ is given by

$$r_{(n-1)n} = \frac{\varepsilon_{fn}\sqrt{\varepsilon_{f(n-1)} - \varepsilon_a \sin^2\varphi_0} - \varepsilon_{f(n-1)}\sqrt{\varepsilon_{f_n} - \varepsilon_a \sin^2\varphi_0}}{\varepsilon_{f_n}\sqrt{\varepsilon_{f(n-1)} - \varepsilon_a \sin^2\varphi_0} + \varepsilon_{f(n-1)}\sqrt{\varepsilon_{f_n} - \varepsilon_a \sin^2\varphi_0}} \quad (4a)$$

and reflectance coefficient from the nth layer to the substrate r_{ns} is given by

$$r_{ns} = \frac{\varepsilon_s\sqrt{\varepsilon_{fn} - \varepsilon_a \sin^2\varphi_0} - \varepsilon_{f_n}\sqrt{\varepsilon_s - \varepsilon_a \sin^2\varphi_0}}{\varepsilon_s\sqrt{\varepsilon_{fn} - \varepsilon_a \sin^2\varphi_0} + \varepsilon_{f_n}\sqrt{\varepsilon_s - \varepsilon_a \sin^2\varphi_0}}. \quad (4b)$$

The phase factor Φ_n for the nth layer is described by

$$\Phi_n = \frac{2\pi d_{fn}}{\lambda}\sqrt{\varepsilon_{fn} - \varepsilon_a \sin^2\varphi_0}. \quad (5)$$

The thickness of the nth film is d_{fn}, φ_0 is the angle of incidence, and ε_a and ε_s are the complex dielectric functions of the ambient and the substrate, respectively. The complex dielectric functions of the $(n-1)^{th}$ and n^{th} films are labeled as $\varepsilon_{f(n-1)}$ and ε_{fn}, respectively. The reflectance amplitude rr_n can be calculated from an $n - 2 \times 2$ matrix multiplication:

$$\begin{bmatrix} M_{11} & M_{12} \\ M_{21} & M_{22} \end{bmatrix} = \begin{bmatrix} 1 & r_{a1} \\ r_{a1} & 1 \end{bmatrix} \times \begin{bmatrix} 1 & r_{12} \\ r_{12}e^{-2j\Phi_1} & e^{-2j\Phi_1} \end{bmatrix} \begin{bmatrix} 1 & r_{23} \\ r_{23}e^{-2j\Phi_2} & e^{-2j\Phi_2} \end{bmatrix} \cdots\cdots \begin{bmatrix} 1 & r_{(n-1)n} \\ r_{(n-1)n}e^{-2j\Phi_n} & e^{-2j\Phi_n} \end{bmatrix} \quad (6)$$

with

$$rr_n = \frac{M_{21}}{M_{11}}. \quad (7)$$

We applied this description to the calculation of the reflectance for a SiO_2-Si_3N_4-SiO_2 multilayer heterostructure on a Si substrate. The calculation reveals discontinuities in the differential reflectivity at the interface of each layer, as shown in Figure 4. First experimental results for SiO_2 and Si_3N_4 film depositions show that the PRS data facilitate the determination of the film thickness, growth rate, and optical constants of deposited films.[18] A more detailed description of real-time PRS monitoring for a specific model system—the growth of GaP on Si(001) by PCBE—follows.

Real-Time PRS Monitoring of GaP PCBE Growth on Vicinal Si(001) Substrates

Figure 5a shows the experimental setup for real-time monitoring of epitaxial GaP deposition on a Si substrate by

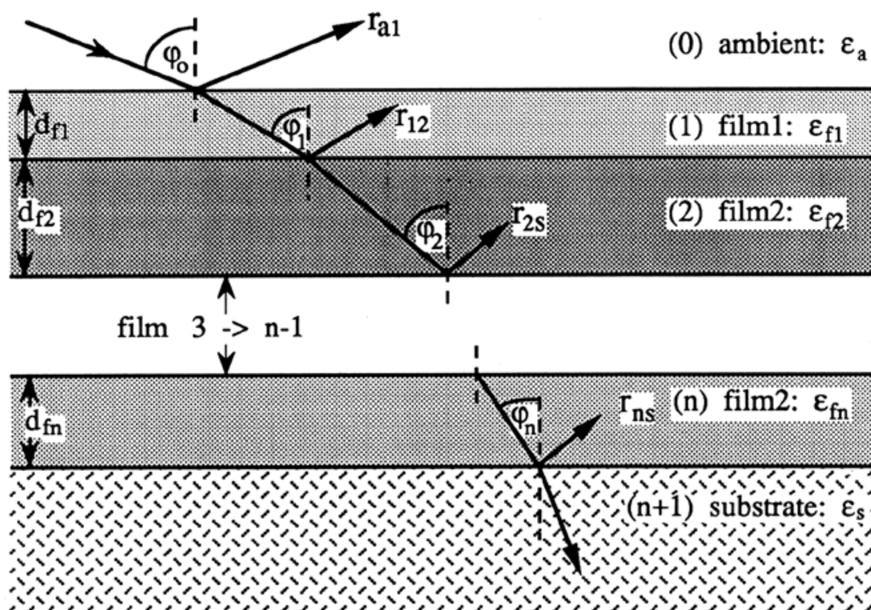

Figure 3. Model description of an n layer system (ambient/film 1) to (film n/substrate) for p-polarized light and homogenous isotropic media.

PRS and reflection high energy electron diffraction (RHEED). We employed a combination of He-Ne laser (λ = 632.8 nm) and a Glan Thompson polarizer to generate a p-polarized beam, impinging on the substrate at an angle of incidence $\varphi = 72°$, close to the Brewster angle of the substrate. The angle of incidence can be adjusted in the range of 3°–5°, which allows a synchronization of *in situ* RHEED with PRS. To minimize errors caused by depolarization,[16] a high-quality, stress-free quartz window at the entrance side of the reactor is employed in combination with a Glan Thompson prism ($R_s/R_p < 10^{-6}$), resulting in an estimated extinction ratio $R_s/R_p < 10^{-5}$. Unlike ellipsometric spectroscopy, PRS does not require special attention to the exit window which might change the polarization state of the reflected light. The reflected beam is detected by a Si photodiode with integrated preamplifier, the output of which is fed into a lock-in amplifier and recorded by a data acquisition system. Simultaneously, scattered radiation is detected by a sensitive photomultiplier tube (PMT) located outside the plane defined by the incident and reflected laser beam. The output of this PMT is routed to a second phase-sensitive amplifier and stored in the data-acquisition system. The randomly scattered radiation contains information on the roughness of the surface as well as substrate/film interface roughening.

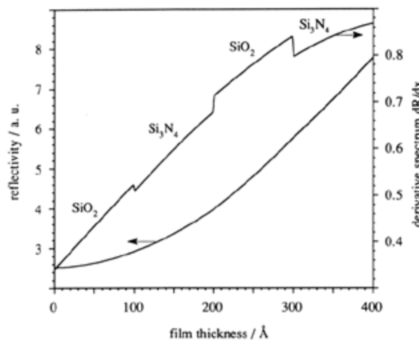

Figure 4. Calculated changes in the reflectivity for SiO_2-Si_3N_4-SiO_2 multilayer deposition on a Si substrate.

The fluxes of the gas sources employed in the deposition process—triethylgallium (TEG), tertiarybutyl phosphine (TBP), and hydrogen—are controlled by mass flow controllers, as schematically shown in Figure 5b. They are directed via computer-controlled three-way valves to either the reactor chamber or a separately pumped bypass chamber,[10,12,19] allowing the sequential exposure of the substrate with individual pulses of the precursor molecules. The time constant of the source pulsing is limited by the three-way valves' response time which is of the order of 0.1–0.2 s. The total gas-flow rate in the chamber is ~5 sccm, which leads to a pressure in the low 10^{-4} mbar range during the deposition. The switching of the sources is synchronized with the data acquisition of the PRS signals to relate observed changes in the reflected intensity of the light to chemistry-induced changes in the optical properties. The Si(001) substrates, misoriented by 4° toward (011), were subjected to a modified RCA cleaning, terminating in a buffered HF dip before loading into the growth chamber. This results in a hydrogen-terminated Si(001) 1 × 1 surface as verified by RHEED before starting the growth procedure. Also, vicinal GaP(001) substrates were cleaned as described previously.[20,21]

Upon initiation of heteroepitaxial growth, the reflected intensity $R_p = rr_p rr_p^*$ oscillates with a period corresponding to quarter-wave film thickness between adjacent minima, as illustrated in Figure 6. Also shown (lower curve) is the intensity of the scattered light as a function of the growth time. During the initial nucleation period of about 150 s, an increase in the intensity of the scattered radiation, as well as in the PRS signal, is observed. After the nucleation period, the intensity of the scattered light evolves steadily and can be correlated to the final surface roughness, observed by *ex situ* atomic force microscopy (AFM). The inserts in Figure 6 show sections of the amplitude-modulated fine structure, which is superimposed on the quarter-wave oscillation in the reflected signal. This fine structure is maintained throughout the entire film growth with a periodicity strongly related to a complete pulse-cycle sequence built up by a TPB pulse of length *a*, followed by a delay *x*, a TEG pulse of length *b*, and a second delay of length *y*. Comparison of the final surface roughness measured by AFM with the chosen pulse-cycle sequences yield best deposition conditions for a pulse-width ratio $a:b = 0.8:0.2$. The flux intensity and the dose ratio TBP:TEG of 0.5:0.06 were kept constant. An ultrapure continuous flux of activated hydrogen is provided during the entire sequence.

In Figure 7, we show the pulse sequence for the TBP and TEG sources with a delay of 3 s ($x:y = 1.2:1.8$ s) and a total cycle time of 4 s. For this condition the growth rate per cycle is estimated to be 3.18 ± 0.1 Å/cycle, assuming a constant growth rate over the entire deposi-

tion process. Varying the delay times between the source pulses in the range of 0.5–6 s results in a variation of the growth rate per cycle ranging from 2 Å/cycle to 3.6 Å/cycle.[10] Accordingly, the observed amplitude-modulated fine structure changes with the change in the growth rate per cycle as shown in Figure 8. It shows the amplitude-modulated periodicity for (a) 2-s, (b) 3-s, and (c) 6-s delays between the source pulses. Both the amplitude modulation of the fine structure and the growth rate per cycle are also affected by changing the fluxes of the precursors (TBP and TEG) for a constant pulse-cycle time sequence. Flux conditions can be found where the amplitude modulation vanishes and only the period fine structure remains.

Under the condition of GaP homoepitaxy, the quarter-wave oscillation vanishes because of the absence of interference, but the amplitude-modulated fine structure remains with the same periodicity as observed for heteroepitaxial growth under the same precursor-cycle condition over the entire growth process. PRS real-time monitoring thus provides information on the growth kinetics for both homo- and heteroepitaxial processes. Figure 9 shows the PRS signal and the intensity of the scattered light for the initial stage of homoepitaxial GaP growth. The same amplitude-modulated fine structure as in the PRS signal is observed in the scattered light, but with inverted intensity, which also follows the periodicity of the precursor-cycle sequence.

In heteroepitaxial processes, the initial stage of nucleation and overgrowth is particularly important for the perfection of the epitaxial film, which is clearly affected by the chosen flux rates, pulse-cycle sequences, and filament-assisted hydrogen flux. Figure 10a shows the PRS signal and the intensity of the scattered light in the initial heteroepitaxial GaP growth period with a pulse-cycle sequence of 2.5 s. After a short incubation period of about 15 s, an enhanced PRS signal can be observed during the nucleation period of about 30 s. As shown in Figure 10b, the increased PRS signal during the nucleation period can be suppressed by an increased TEG flux during the first 100 s of growth with an otherwise identical growth condition.

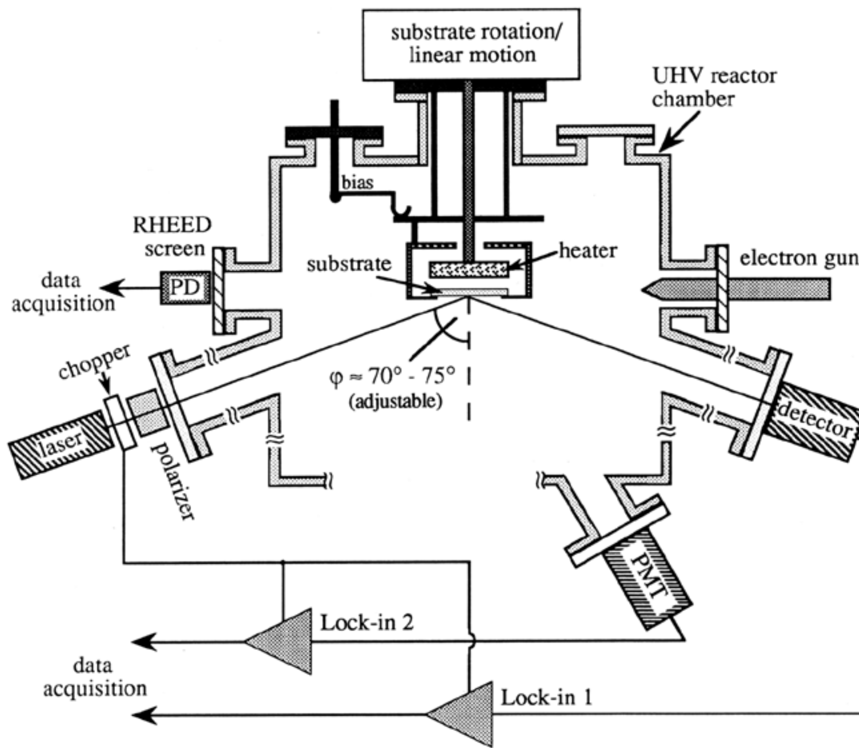

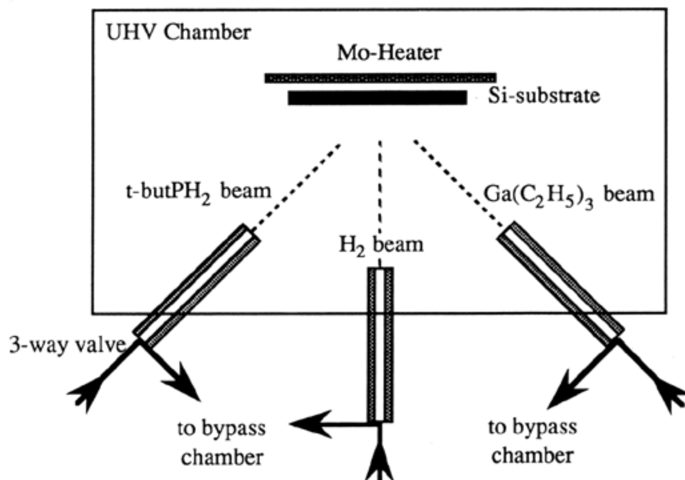

Figure 5. (a) Schematic representation of the experimental setup for the PRS experiment and (b) schematic representation of a system for PCBE.

Discussion

Detailed information regarding the nucleation and epitaxial overgrowth process is obtained from the analysis of the fine structure that is superimposed on the quarter-wave oscillations of the reflected intensity. It relates to modifications of the optical properties in the vicinity of the surface of the evolving layer because of the exposure to the sequential TEG and t-butPH$_2$ (TBP) pulses. Each peak in the fine structure represents a complete precursor cycle. In contrast to RHEED oscillations, the fine structure is maintained for thousands of cycles. Thus PRS permits the following of the homo- and heteroepitaxial growth processes with submonolayer resolution over the thousands of angstroms of film growth, thus providing access to the study of the growth mechanism in both the nucleation and initial growth phase,

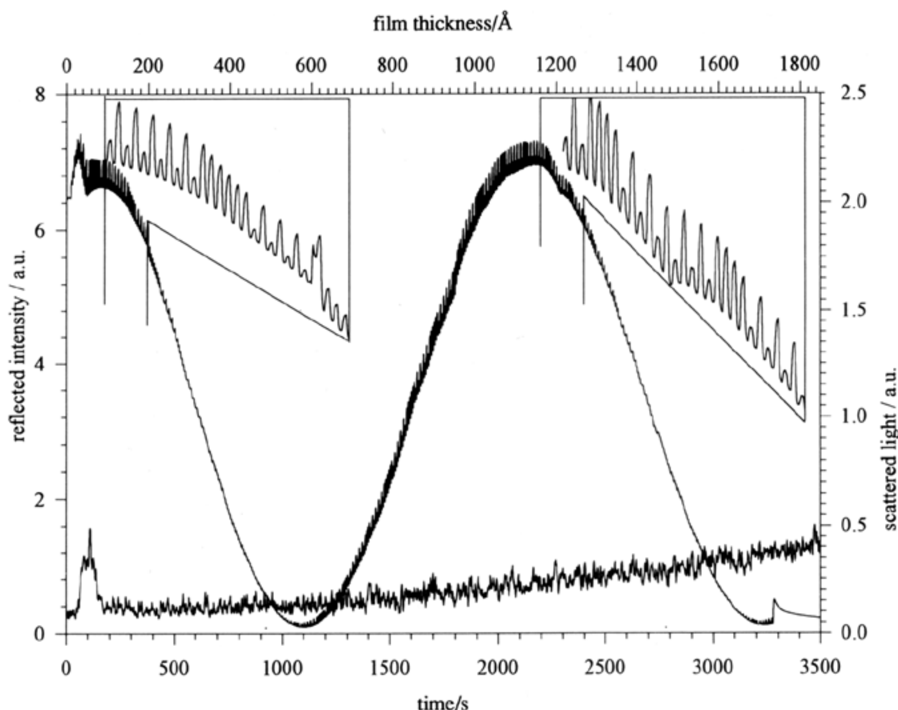

Figure 6. PRS signal (upper curve with two enlarged inserts) and scattered light intensity (lower curve) for heteroepitaxial film growth of GaP on Si(001) at 310°C with a delay time between the source pulses of 6 s.

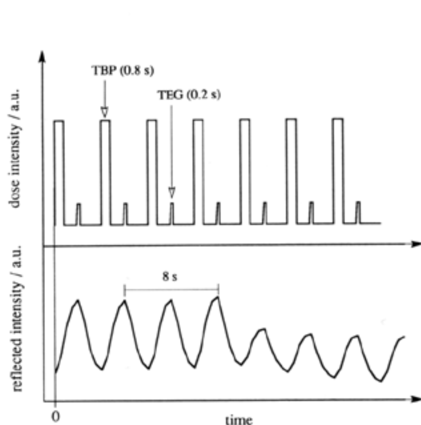

Figure 7. Correlation of the TBP and TEG pulse sequences (top) with the corresponding oscillations in the PRS signal for a delay time between the source pulses of 3 s.

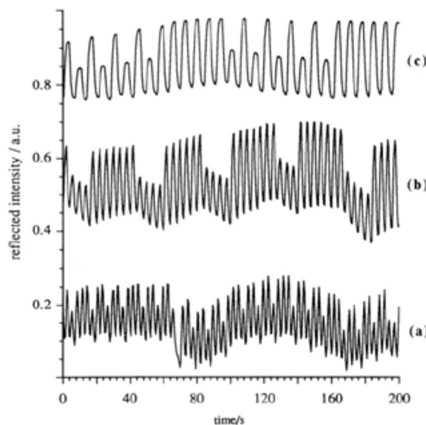

Figure 8. Variation in the amplitude-modulated fine structure in the PRS signal for (a) 2-s, (b) 3-s, and (c) 6-s delay times between the source pulses for heteroepitaxial growth of GaP on Si(001) at 310°C.

as well as in the later stages of film growth. In the case of homoepitaxy, the quarter-wave oscillations in the reflected intensity do not exist, but the fine structure persists. This fine structure might be related to observations made by SPA, previously described in the context of GaAs-based homoepitaxial structures under the conditions of molecular beam epitaxy (MBE).[6,22] However, a difference exists between SPA and PRS as SPA chooses a probe light energy well above the absorption edge to gain high surface sensitivity, while in PRS the wavelength is not limited to above bandgap radiation. This allows the sensing for both bulk and surface contributions. Therefore, it is not clear at present whether or not the observed oscillations in the SPA signal, which are only reported during the initial growth period, are related to the same physical phenomena observed in the PRS spectra. The amplitude modulation in the fine structure indicates contributions of several monolayers to the observed changes in the reflected signal. Out of the periodicity of the amplitude modulation and the growth rate per cycle, we can estimate an information/signal depth of 20–30 Å. A model description for the fine structure thus needs to include at least two contributions: (1) a subsurface layer of the order of several monolayers, which includes surface morphology and/or surface reconstruction information and (2) a surface (sub)monolayer describing the chemically bonded precursor radicals which modify the surface dielectric function. Both contributions should show a wavelength dependence, which may allow separation of the effects.

The fine structure in the PRS observed under the homoepitaxial growth condition permits calibration of the layer thickness deposited per precursor cycle on the basis of the quarter-wave oscillations observed in a heteroepitaxial growth experiment under the same growth conditions. In the case of GaP epitaxy on Si(001) by PCBE, the layer thickness deposited per precursor cycle does not change from the initial overgrowth phase to the completion of the film growth.[12] As shown in Figures 6, 8, and 9, the growth rate per pulse-cycle sequence can be affected by the pulse width and delays in the cycle sequence and the fluxes of the precursor. However, the observed growth rate per pulse-cycle sequence shows a saturation of the order of 3.8 Å per cycle. This raises the question as to whether or not PCBE permits the achievement of an atomic-layer growth mode.

Epitaxial GaP films grown on silicon by chemical beam epitaxy (CBE) contain planar defects that are related to the three-dimensional island formation of GaP during the nucleation phase on the silicon substrate.[13,23] The GaP nuclei tend to grow out into three-dimensional islands because of two independent causes: (1) The habit of the nuclei is thermodynamically defined by the modified Wulff's law. (2) The pyrolysis of TBP on the surface of the GaP nuclei is catalytically enhanced compared to the bare Si surface.

High resolution transmission electron microscopy (HRTEM) and AFM support the mechanisms of three-dimensional nucleation and stacking-fault formation of GaP on Si.[13,24] Heteroepitaxial growth without filament-assisted hydrogen provided AFM scans with surface morphology that represent a growth mechanism with nucleation facets along the [111] planes.[13] The initial, clean silicon surface measured by AFM yields an rms surface roughness of 5 Å. The AFM image for a sample with 20 s of GaP growth shows three-dimensional nucleation islands with an rms surface roughness of 19 Å. After 40 s of growth, a contiguous film formed with an rms surface roughness of 1 nm. Extended growth does not roughen the surface to a final rms value that is significantly more than that of the initial nucleation stage.

Additional insights into the nucleation process are gained from the real-time monitored results obtained by PRS and scattered light intensities.[12] As shown in Figure 6, a substantial enhancement in both the reflected and scattered intensity during the nucleation period is observed. The increased reflected intensity during the initial growth period indicates an apparently larger difference in the dielectric functions between film and substrate than in the later stage of film growth. This can be explained by corrugations in the surface during the initial growth period, which requires the replacement of the dielectric function for the bulk film by an effective dielectric function:

$$\varepsilon_{\mathrm{eff}} = \varepsilon_a \frac{\varepsilon_f(1 + 2q) + \varepsilon_a(1 - q)}{\varepsilon_f(1 - q) + \varepsilon_a(2 + q)} \qquad (8)$$

which describes the corrugation of the surface through the corrugation parameter q, varying between $0 \leq q \leq 1$ as the film develops from ambient ($q = 0$) to contiguous film coverage ($q = 1$). Therefore, during partial coverage of the surface, the effective dielectric function is smaller than that of the contiguous film thus explaining the observed higher reflectance during the nucleation stage. The excess amplitude of the PRS signal during the nucleation period can be related to the degree of deviation from two-dimensional growth. That is, depending on the surface conditioning/growth conditions, we have observed variation from pronounced three-dimensional behavior to nearly two-dimensional nucleation and overgrowth. For example, Figure 10a shows PRS intensity during the growth period, clearly revealing an increased PRS signal during the initial period of nucleation. With the same *ex situ* cleaning steps and the same preconditioning (heat-up cycles), a modified cycle sequence of TEG and TBP fluxes results in a nearly two-dimensional nucleation mechanism as shown in Figure 10b. The various effects causing deviations in the PRS signal, as predicted from model considerations based on ideal homogenous isotropic dielectrics, are at present not completely known. Therefore, further efforts in the mathematical modeling must incorporate a variety of effects that modify the PRS response, such as:

- the temperature dependence of the dielectric functions,

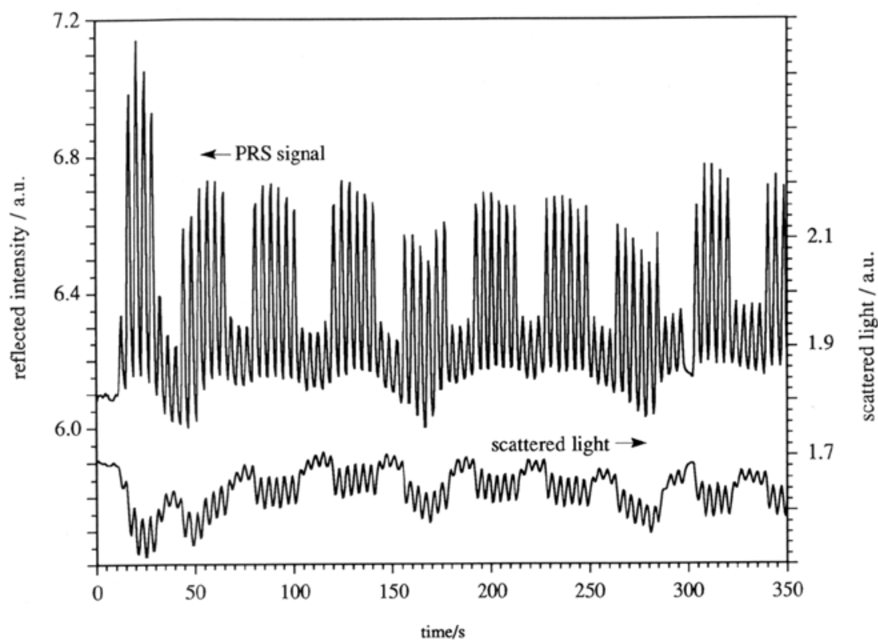

Figure 9. Changes in the amplitude-modulated fine structure of the PRS signal and correlated changes in the intensity of the scattered radiation during the initial phase of homoepitaxial growth of GaP on vicinal GaP(001) at 310°C.

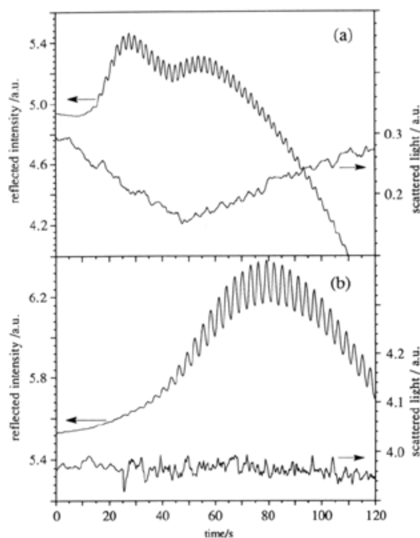

Figure 10. Changes in the PRS signal and in the intensity of the scattered radiation during the initial heteroepitaxial growth period of GaP on Si(001) at 350°C: (a) standard growth conditions with a pulse-cycle sequence of 2.5 s and (b) same growth condition with an increased TEG flux during the initial growth time.

- surface roughening with microscopic scattering mechanisms,
- interfacial roughening (substrate/film or (layer $x + 1$)/(layer x)),
- surface-chemistry-induced modification and formation of a subsurface layer which describes the superimposed fine structure, and
- absorption in the layer because of point-defect formation which may or may not result in deviations from the ideal stoichiometric atom ratio in the film.

Conclusion

We applied PRS to monitor homo- and heteroepitaxial growth processes under the condition of PCBE, showing that PRS allows precise measurements of the film thickness and the optical constants. The high sensitivity of this method permits the observation of an amplitude-modulated fine structure, which provides an angstrom-scale periodicity over thousands of angstroms of film growth. This periodicity can be used for a better understanding of the surface chemistry and topography during the deposition process. The growth-process conditions thus can be optimized toward conditions where the amplitude modulation vanishes with a remaining period fine structure which follows the cycle sequence of the precursor. Although the quarter-wave oscillations associated with heteroepitaxial film growth are lost, the amplitude-modulated fine structure is maintained under the condition of homoepitaxial growth, allowing real-time assessment of the growth rate in homoepitaxial processes. Under a condition of PCBE, the deposition process and the surface chemistry can be engineered and optimized by tuning the pulse width and delay times in the cycle sequence and the fluxes of the precursor, forcing the heteroepitaxial nucleation toward the two-dimensional growth condition.

Extension of the applications of PRS to other deposition processes will allow for the exploration of spectroscopic or multicolor PRS, where each selected wavelength probes a different area of interest, such as surface, substrate/film interface, or bulk properties of the growing heterostructure. This is expected to allow separation of the depth-dependent contributions near the surface and interfaces and the correlation to structural, optical, and electrical properties of the grown layer. Correlation of the PRS signal to other *ex situ* and *in situ* measurements is essential for the creation of a database for both theoretical simulation of growth kinetics and definition of process parameters that may be utilized for closed-loop control of the deposition process. This development mandates—in addition to progress in hardware design and process engineering—the generation of fast, real-time process simulation codes and advanced control theory. Such developments require close interaction and input from applied mathematics and materials-research groups.

Acknowledgments

This work has been supported by the National Science Foundation grant DMR 9820022 and AFOSR grant F48620-94-1-0447.

References

1. J.V. Armstrong, T. Farrell, T.B. Joyce, P. Kightley, T.J. Bullough, and P.J. Goodhew, *J. Cryst. Growth* **120** (1992) p. 84.
2. K.P. Killeen and W.G. Breiland, *J. Electron. Mater.* **23** (2) (1993) p. 279.
3. H. Grothe and F.G. Boebel, *J. Cryst. Growth* **127** (1993) p. 1010.
4. D.E. Aspnes, J.P. Harbison, A.A. Studna, and L.T. Florez, *Appl. Phys. Lett.* **52** (12) (1988) p. 957.
5. D.E. Aspnes, *Proc. SPIE* **1285**, edited by Anupam Madhukar (International Society of Optical Engineers, 1990) p. 2.
6. N. Kobayashi and Y. Horikoshi, *Jpn. Appl. Phys.* **28** (11) (1989) p. L1880.
7. Y. Horikoshi, *Prog. in Cryst. Growth and Characterization of Mater.* **23** (1992) p. 73.
8. D.E. Aspnes, W.E. Quinn, and S. Gregory, *Appl. Phys. Lett.* **56** (25) (1990) p. 2,569.
9. D.E. Aspnes, W.E. Quinn, and S. Gregory, *J. Vac. Sci. & Technol. A* **9** (3) (1991) p. 870.
10. N. Dietz, A.E. Miller, J.T. Kelliher, D. Venables, and K.J. Bachmann, *J. Cryst. Growth* in press.
11. N. Dietz, A.E. Miller, and K.J. Bachmann, *J. Vac. Sci. Technol. A* **13** (1995) p. 153.
12. K.J. Bachmann, N. Dietz, A.E. Miller, D. Venables, and J.T. Kelliher, *J. Vac. Sci. Technol. A* **13** (3) in press.
13. A.E. Miller, J.T. Kelliher, N. Dietz, and K.J. Bachmann, in *Evolution of Thin-Film and Surface Structure and Morphology*, edited by B.G. Demczyk, E.D. Williams, E. Garfunkel, B.M. Clemens, and J.E. Cuomo (Mat. Res. Soc. Symp. Proc. **355**, Pittsburgh, 1995).
14. S.P.F.b.t.l. Humphreys-Owen, *Proc. Phys. Soc.* **77** (1961) p. 949.
15. N. Dietz and H.J. Lewerenz, *Appl. Phys. Lett.* **60** (19) (1992) p. 2,403.
16. N. Dietz and H.J. Lewerenz, *Appl. Surf. Sci.* **69** (1993) p. 350.
17. R.M.A. Azzam, *Appl. Optics* **22** (24) (1983) p. 4,155.
18. N. Dietz, D.J. Stephens, G. Lucovsky, and K.J. Bachmann, in *Diagnostic Techniques for Semiconductor Materials Processing*, edited by O.J. Glembocki, S.W. Pang, F.H. Pollak, G.M. Crean, and G. Larrabee (Mater. Res. Soc. Symp. Proc. **324**, Pittsburgh, 1994) p. 27.
19. J.T. Kelliher, J. Thornton, N. Dietz, G. Lucovsky and K.J. Bachmann, *Mat. Sci. & Eng. B* **22** (1993) p. 97.
20. Z. Lu, S. Habermehl, G. Lucovsky, N. Dietz, and K.J. Bachmann, in *Proc. 3rd Int. Symp. on Cleaning Technol. in Semiconductor Device Manufacturing* **94–7** (New Orleans, 1994) p. 416.
21. S. Habermehl, N. Dietz, Z. Lu, K.J. Bachmann, and G. Lucovsky, *J. Vac. Sci. Technol. A* **12** (4) (1994) p. 990.
22. N. Kobayashi, T. Makimoto, Y. Yamauchi, and Y. Horikoshi, *J. Cryst. Growth* **107** (1–4) (1991) p. 62.
23. P. Pirouz, F. Ernst, and T.T. Cheng, in *Heteroepitaxy on Silicon: Fundamentals, Structures, and Devices*, edited by H.K. Choi, R. Hull, H. Ishiwara, and R.J. Nemanich (Mater. Res. Soc. Symp. Proc. **116**, Pittsburgh, 1988) p. 57.
24. F. Ernst and P. Pirouz, *J. Appl. Phys.* **64** (9) (1988) p. 4,526. □